



Pergamon

Acta mater. 49 (2001) 2827–2841



www.elsevier.com/locate/actamat

ON THE ORIGIN OF THE HIGH COARSENING RESISTANCE OF Ω PLATES IN Al–Cu–Mg–Ag ALLOYS

C. R. HUTCHINSON¹, X. FAN^{2, 3}, S. J. PENNYCOOK³ and G. J. SHIFLET^{1†}

¹Department of Materials Science and Engineering, University of Virginia, Charlottesville, VA 22903, USA, ²Department of Chemical and Materials Engineering, University of Kentucky, Lexington, KY 40506, USA and ³Solid State Division, Oak Ridge National Laboratory, Oak Ridge, TN 37831, USA

(Received 20 February 2001; received in revised form 8 March 2001; accepted 2 April 2001)

Abstract—The thickening kinetics of Ω plates in an Al–4Cu–0.3Mg–0.2Ag (wt. %) alloy have been measured at 200, 250 and 300°C using conventional transmission electron microscopy techniques. At all temperatures examined the thickening showed a linear dependence on time. At 200°C the plates remained less than 6 nm in thickness after 1000 h exposure. At temperatures above 200°C the thickening kinetics are greatly increased. Atomic resolution Z-contrast microscopy has been used to examine the structure and chemistry of the (001)_Ω|| (111)_α interphase boundary in samples treated at each temperature. In all cases, two atomic layers of Ag and Mg segregation were found at the broad face of the plate. The risers of the thickening ledges and the ends of the plates were free of Ag segregation. The necessary redistribution of Ag and Mg accompanying a migrating thickening ledge occurs at all temperatures and is not considered to play a decisive role in the excellent coarsening resistance exhibited by the Ω plates at temperatures up to 200°C. Plates transformed at 200°C rarely contained ledges and usually exhibited a strong vacancy misfit normal to the plate. A large increase in ledge density was observed on plates transformed at 300°C, concomitant with accelerated plate thickening kinetics. The high resistance to plate coarsening exhibited by Ω plates at temperatures up to 200°C, is due to a prohibitively high barrier to ledge nucleation in the strong vacancy field normal to the broad face of the plate. Results also suggest that accommodation of the large misfit that exists normal to the broad face of the plate is unlikely to provide the driving force for Ag and Mg segregation. © 2001 Acta Materialia Inc. Published by Elsevier Science Ltd. All rights reserved.

Keywords: Aluminium; Phase transformations; Interface; Segregation; Z-contrast microscopy

1. BACKGROUND

The addition of trace amounts (<0.1 at. %) of an alloying element to selected age hardenable Al-alloys can have a marked effect on mechanical properties. One such trace element to receive considerable attention is Ag. The effect of Ag was first reported in 1960 [1] where its addition to Al–Zn–Mg based alloys enhanced the response to age hardening through a refinement of the precipitate dispersion. Further work on the addition of Ag to other precipitation hardened Al-alloy systems generalized the beneficial influence to all Al-alloys containing Mg [2]. The phenomenon was attributed to an interaction between Ag and Mg atoms and the subsequent effect on the nucleation of intermediate precipitates. In alloy systems such as Al–Cu–Mg with high Cu:Mg ratios (e.g., 10:1), the addition not only enhanced the hardening response but totally changed the precipitation processes usually

observed in these alloys [3–6]. The Ag addition promoted the formation of a fine and uniform dispersion of hexagonal-shaped plate-like precipitates on the {111}_α planes of the matrix at the expense of the precipitation of θ' (Al₂Cu) which is usually observed in these alloys. This new phase was designated Ω .

Alloys based on the Al–Cu–Mg–Ag system exhibit superior strength and creep resistance and these desirable properties are attributed to the fine and uniform distribution of Ω and its excellent thermal stability at temperatures up to 200°C [7]. The high resistance of Ω to plate coarsening has led to the development of at least two new compositions based on the Al–Cu–Mg–Ag system [8, 9]. One proposed application for an Al–Cu–Mg–Ag alloy, strengthened predominantly by the Ω phase, is in the fuselage of a new supersonic transport aircraft that may replace the Concorde early this century [10]. Several structures for the Ω phase have been proposed [11–15] although the most widely accepted structure is orthorhombic (Fmmm, $a = 0.496$ nm, $b = 0.859$ nm, $c = 0.848$ nm) [16, 17]. The orientation relationship between Ω and the Al matrix is (111)_Ω|| (001)_{Al} and [110]_Ω|| [010]_{Al}. The

†To whom all correspondence should be addressed.
Tel.: +1-804-982-5653; Fax: +1-804-982-5660.
E-mail address: gjs@virginia.edu (G. J. Shiflet)

orthorhombic structure for Ω is assumed throughout this paper. There is little difference between each of the proposed structural models and the equilibrium tetragonal θ phase (14/mcm, $a = b = 0.6066$ nm, $c = 0.4874$ nm) which forms in overaged binary Al–Cu alloys. This similarity was first recognized by Auld [11, 12] and led him to designate the $\{111\}_\alpha$ precipitate θ_M , a modified version of θ . Garg *et al.* [15] later adopted a similar designation, θ_M , for their proposed model. Although rarely observed, a variant of the equilibrium θ phase is reported to form on the $\{111\}_\alpha$ planes in the binary Al–Cu system. It is referred to as the Vaughan II orientation [18]. Until recently the mechanism of how Ag and Mg promote the nucleation of Ω has been a matter only of speculation. Several precursor phases [4, 19] and heterogeneous nucleation sites [13] were proposed over the years but each lacked widespread verification [20–23]. The results of a recent three-dimensional atom probe field ion microscopy (3D-APFIM) study by Reich *et al.* [38] were interpreted as experimental evidence suggesting the Ω phase evolves continuously from co-clusters containing Ag and Mg aligned on $\{111\}_\alpha$ planes of the matrix. Hono *et al.* [24] first reported the observation of co-clusters of Ag and Mg in these alloys, but at that stage it wasn't clear how the clusters facilitated the nucleation of Ω . The observations of Reich *et al.* [38] are supported by the theoretical calculations of Suh and Park [25] who predict that co-clusters of Ag and Mg in an Al matrix will elongate along $\{111\}_\alpha$ planes to minimize their strain energy. The interfacial structure of well developed Ω plates was addressed by Garg *et al.* and a growth model for Ω proposed [26]. Concerning the stability of Ω , the phase is observed to form in Al–Cu–Mg–Ag alloys at temperatures up to 470°C [27]. However, investigations of long term stability have provided inconsistent results and unequivocal evidence concerning the equilibrium or metastable nature of the Ω phase is lacking [3, 6, 12, 27, 28].

2. INTRODUCTION

The desirable strength and creep properties that alloys based on the Al–Cu–Mg–Ag system exhibit are attributed to the fine, uniform and thermally stable distribution of Ω precipitates that form on the matrix $\{111\}_\alpha$ planes [7]. This paper is concerned with contributing to an understanding of the origin of the reported high coarsening resistance of Ω plates at temperatures up to 200°C. The reported coarsening resistance was confirmed by Ringer *et al.* [28]. Those researchers directly measured the changes in plate thickness using conventional transmission electron microscopy (CTEM) techniques as a function of time for temperatures between 200 and 300°C. The Ω plates examined in that study remained less than 6 nm in thickness after aging for 1000 h at 200°C. At temperatures above 200°C, the thickening was greatly

accelerated, with thicknesses in excess of 30 nm being reached within 50 h exposure at 300°C (Fig. 1).

2.1. Overall plate thickening kinetics

It is now generally accepted that rationally oriented plate-like precipitates thicken by a ledge mechanism [29]. Several studies on precipitate plate thickening kinetics in Al-alloys have been reported. These include θ' in Al–Cu alloys [30, 31] and γ in Al–Ag alloys [32]. In each case, the overall thickening kinetics were somewhat slower than allowed by volume diffusion of the solute, indicating an interface controlled mechanism. It was concluded that while the migration rate of individual ledges is in good agreement with diffusion controlled migration, the overall thickening kinetics are restricted by a limited supply of ledges [30–34].

2.2. Ledge nucleation and strain state

The importance of elastic strain in the morphological development of precipitate plates has been highlighted by several authors. Stobbs and Purdy [35] reported that θ' plates form only with certain discrete thicknesses, which consist of specific multiples of θ' half unit cells. Each thickness being associated with a particular lattice strain normal to the habit plane of the plate, either vacancy or interstitial (Fig. 2). Dahmen and Westmacott's analysis [36] of these results showed that the observed thicknesses are characterized by a minimization of both shape and volume strains. Fonda *et al.* [37] extended these ideas to the accommodation of misfit strain normal to the habit plane of Ω plates in Al–Cu–Mg–Ag alloys. Among plate-like precipitates that form on $\{111\}_\alpha$ planes of the Al matrix, Ω is somewhat of an anomaly. Other examples include T_1 (Al_2CuLi) in Al–Cu–Li alloys, η' ($MgZn_2$) in Al–Mg–Zn and γ' ($AlAg_2$) in Al–Ag. Each of these phases has a hexagonal crystal structure

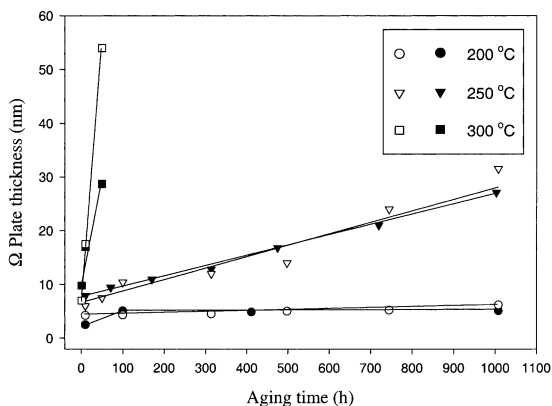


Fig. 1. Mean Ω plate thickness as a function of time (h) at 200°C, 250°C and 300°C. Full symbols are for the Al–4Cu–0.3Mg–0.4Ag (wt. %) alloy used in this study. The data points at early times for samples treated at 200°C are 10 and 100 h, at 250°C the early times are 10 and 70 h and at 300°C, 1, 10 and 50 h. Open symbols are for an Al–6.5Cu–0.45Mg–0.4Ag–0.5Mn–0.2Zr (wt. %) alloy studied by Ringer *et al.* [28].

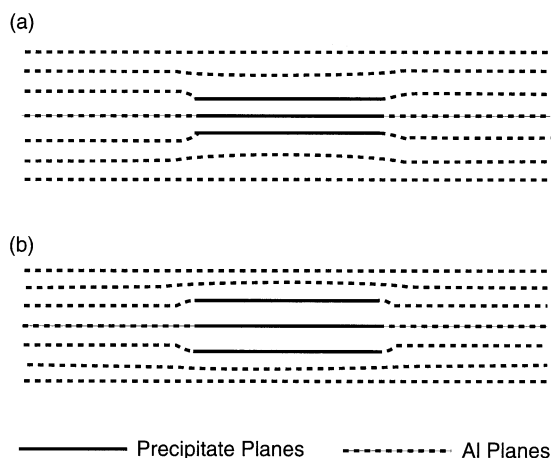


Fig. 2. Schematic illustration of (a) vacancy and (b) interstitial strain fields normal to the broad face of a precipitate plate.

whereas Ω is usually assumed to be orthorhombic. The misfit normal to the precipitate for each of these phases is 0.12% for T_1 , 0.03% for η' , 1.46% for γ' and 9.3% for Ω . The misfit normal to the Ω plate is accordingly considered large. On the basis of this large misfit, Fonda *et al.* [37] initially postulated that the source of the enhanced thermal stability of Ω may be the relationship between ledge nucleation and propagation and the elastic strain field. Fonda *et al.* [37] investigated the accommodation of misfit strain surrounding Ω plates and found the plates consistently exhibit a vacancy type strain field normal to the habit plane, independent of plate thickness. Two types of thickening ledges were observed, coherent $1/2$ Ω unit cell high ledges and less commonly, larger ledges which contain a misfit compensating dislocation of the type $\mathbf{b} = 1/3\langle 111 \rangle_{\alpha}$. Similar dislocations were also observed at the ends of the plates with an average spacing of $2 \frac{1}{2}$ or 3Ω unit cells, which produces a minimum strain normal to the plate.

2.3. Ledge migration and solute redistribution

The 3D-APFIM work of Reich *et al.* [38] has provided evidence to warrant careful consideration of the usual assumption that ledge nucleation controls the overall plate thickening rate in Al-based alloys. In Reich *et al.*'s [38] atom probe study, they captured an Ω plate thickening ledge in an Al-1.9Cu-0.3Mg-0.2Ag (at. %) alloy aged 10 h at 180°C. Their observations show the presence of a monoatomic layer of Ag and Mg at the Ω plate/matrix $(001)_{\Omega} \parallel (111)_{\alpha}$ interface but no Ag or Mg was detected within the plate itself or at the riser of the ledge. The association of Ag and Mg with Ω plates is well documented with both analytical transmission electron microscopy (ATEM) and atom probe field ion microscopy techniques (APFIM) (Table 1). Most investigations support the observations of Reich *et al.* [38]. The motion of the thickening ledge must then involve the simultaneous flux of Cu from the matrix to the riser of the ledge and the redistribution of Ag and Mg from the

original broad face of the Ω plate to the terrace of the migrating thickening ledge. Figure 3 is a schematic illustration of this process[†]. This complicated diffusion geometry raises two interesting questions. (a) What interaction (if any) is there between the redistributing Ag and Mg and the incoming flux of Cu? and (b) If an interaction is expected, could it be sufficient to retard ledge migration to the point where it becomes the rate controlling process for plate thickening instead of ledge nucleation?

APFIM studies of early stages of decomposition of supersaturated Al-Cu-Mg alloys revealed evidence of co-clustering of Cu and Mg on the FCC lattice [23, 39], suggesting a preferred interaction between these elements. This is not surprising considering the Gibbs free energy of mixing for the FCC phase in the Cu-Mg system exhibits a negative departure from ideal behavior [40]. The redistributing Mg may be expected to retard the flux of Cu through such an interaction and slow ledge migration. APFIM studies of the decomposition of Al-Cu-Mg-Ag alloys revealed Ag and Mg also exhibit strong co-clustering tendencies [23, 24, 38, 41], but no preferred interactions between Ag and Cu are reported. The Gibbs free energy of mixing for the FCC phase in the Ag-Cu system exhibits a positive deviation from ideal behavior [21] indicating a tendency for Ag and Cu atoms to resist mixing on the FCC lattice. The effect of the necessary redistribution of Ag and Mg near/at the ledge riser on the Cu flux is not obvious. Under these circumstances, an investigation of the role of ledge migration, rather than ledge nucleation, in the coarsening resistance of Ω plates at temperatures up to 200°C is warranted. Furthermore, the great majority of analytical investigations of Ω plates are on plates formed at 200°C or below (Table 1). This is the temperature regime where the plates exhibit excellent coarsening resistance (Fig. 1). There is a relative paucity of data concerning the segregation behavior of Ag and Mg at temperatures above 200°C where thickening is greatly enhanced.

The present work addresses the need for a systematic study of the structure and chemistry of the Ω plate/matrix $(001)_{\Omega} \parallel (111)_{\alpha}$ interface as a function of time and temperature to examine the respective roles of ledge nucleation and migration in accounting for the excellent coarsening resistance of Ω plates at temperatures up to 200°C.

3. EXPERIMENTAL PROCEDURE

The nominal composition of the alloy used in this study is Al-4.0Cu-0.3Mg-0.4Ag (wt. %). Strips of

[†] The diffusion path for Ag and Mg redistribution from the broad face of the plate to the terrace of the migrating thickening ledge shown in Fig. 3 is only one of several possible diffusion paths. This schematic is not intended to imply that this is the path of solute redistribution, only that some interaction between the flux of Cu and the Ag and Mg may be expected.

Table 1. Summary of published research concerning the association of Ag and Mg atoms with Ω precipitates. Observations are listed in chronological order

Alloy Composition (wt. %)	Heat treatment condition	Analytical technique used	Ag or Mg detected inside Ω	Ag or Mg detected at Ω /matrix interface	Ref.
Al-4Cu-0.3Mg-0.4Ag	200°C, 2 h, 10 h	TEM/EDS	(Ag)	(Ag)	[17] ^a
Al-6Cu-0.45Mg-0.5Ag-0.5Mn-0.14Zr	Air cool from 500°C	TEM/EDS	No	Ag, (Mg)	[17] ^b
Al-4Cu-0.3Mg-0.4Ag	170°C, 24 h	POSAP ^c	Mg, Ag	No evidence of pref. seg.	[65]
Al-4Cu-0.3Mg-0.4Ag	170°C, 24 h	POSAP	Mg, Ag	No evidence of pref. seg.	[66]
Al-6Cu-0.45Mg-0.5Ag-0.5Mn-0.14Zr	190°C, 8 h	ToF-AP ^d	No	Ag, Mg	[67]
Al-4.3Cu-0.3Mg-0.8Ag	190°C, 2 h, 8 h	ToF-AP	No	Ag, Mg	[68]
Al-4Cu-0.5Mg-0.5Ag	250°C, 6 min	TEM/EDS	Mg	Ag, Mg	[69]
Al-3.9Cu-0.3Mg-0.4Ag	200°C, 1000 h	TEM/EDS	No	Ag, Mg	[70]
Al-4.3Cu-0.3Mg-0.8Ag	180°C, 2 h, 10 h	3D-APFIM	No	Ag, Mg	[38]

^a For this treatment the Ω plate was ~ 10 nm in thickness and the electron probe diameter was ~ 20 nm. It is unclear whether the Ag is associated with the interface or bulk plate.

^b Mg was detected in association with the Ω plate using EDS in an SEM using deeply etched samples.

^c POSAP: Position Sensitive Atom Probe.

^d ToF-AP: Time-of-Flight Atom Probe.

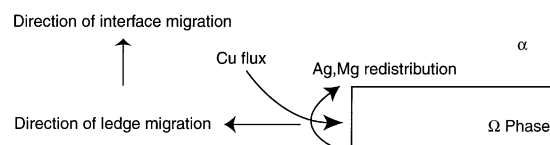


Fig. 3. Schematic illustration of the necessary Ag and Mg redistribution and Cu flux accompanying the migration of a thickening ledge on an Ω plate.

material 0.5–1 mm thick were solution treated (ST) at 525°C for 1 h, water quenched (WQ) and aged in molten salt baths at 200 \pm 2°C, 250 \pm 2°C and 300 \pm 2°C for various times up to 1000 h.

Specimens for transmission electron microscopy (TEM) were punched mechanically from the strips and twin-jet electrolytically polished in a solution of 33 vol. % nitric acid and 67 vol. % methanol at -25°C . The microstructural evolution was monitored using CTEM techniques with a 200 kV microscope. High resolution phase contrast microscopy was performed using a top entry HREM operating at 400 kV. The high resolution phase contrast simulation was performed using the Crystalkit and MacTempas software packages [42]. Atomic resolution Z-contrast microscopy [43–45] was used for the systematic examination of the composition and structure of the Ω plate/matrix $(001)_\Omega \parallel (111)_\alpha$ interface as a function of time and temperature. This technique is capable of providing two-dimensional intuitively interpretable images of atomic structures with compositional sensitivity without the need for model structures and simulations associated with the phase contrast imaging techniques. A Z-contrast image is formed by scanning an electron probe of atomic dimensions across a specimen and collecting the high angle scattered electrons with an annular dark-field (HAADF) detector.

Since the scattering is incoherent at high scattering angles, the image is essentially a map of the total scattering intensity of each atomic column, which is approximately proportional to the square of the atomic number (Z). This technique is especially well suited to the investigation of Ag in the Al–Cu–Mg–Ag system due to the relatively high atomic number of Ag. The microscopy was performed using a VG Microscope HB603U scanning transmission electron microscope operating at 300 kV which is capable of forming an electron probe size of 0.126 nm. Maximum entropy image analysis [46, 47] was applied to enhance the resolution and determine the positions of each atomic column in the images[†]. The EDS analysis was carried out using a ATEM operating at 200 kV equipped with a field emission gun and an EDSX system. For all EDS spectra acquisition, a nominally 1 nm probe was used.

Measurements of the thickness of Ω precipitate plates were made from CTEM micrographs recorded with the electron beam parallel to the precipitate habit plane (i.e. parallel to $\langle 112 \rangle_\alpha / [100]_\Omega$ or $[110]_\Omega$). In each case, the “edge-on” thickness of between 70 and 100 precipitates was measured from the negatives magnified using a 4 \times graticule.

[†] As a result of the spatial incoherence in the transverse plane, Z-contrast imaging can be described in terms of a convolution between an object function (the real space map of the columnar scattering intensity to high angles) and the effective probe. The maximum entropy method calculates the most likely object function that, when convoluted with the effective probe, best matches the experimental data. The probe profile is the only additional information required by the program.

4. RESULTS

4.1. Conventional transmission electron microscopy (CTEM)

Observations of the $\langle 100 \rangle_\alpha$, $\langle 110 \rangle_\alpha$ and $\langle 112 \rangle_\alpha$ zone axes of the Al matrix were made to ensure a true representation of the precipitate distribution was obtained. At all times and temperatures examined, the Ω phase was found to be present. At 200°C and 250°C, the Ω phase co-exists with θ' (Al_2Cu) and S (Al_2CuMg) phases. At 300°C, the Ω phase was the only precipitate found at all times observed. A typical microstructure containing predominately Ω phase is shown in Fig. 4. In this orientation two $\{111\}_\alpha$ planes are aligned parallel to the electron beam and two inclined to the beam. The variants of Ω formed on the $\{111\}_\alpha$ planes parallel to and inclined to the beam can clearly be resolved. Some θ' and S phase precipitates are also visible in this micrograph.

The thickening kinetics of Ω plates were measured at 200, 250 and 300°C. The Ω plate thickness is plotted as a function of time in Fig. 1. At all temperatures examined the precipitate thickness shows a linear dependence on time. At 200°C, the Ω plates reach a thickness of approximately 5.5 nm after 100 h exposure, after which there is no detectable change in average thickness. At 300°C the rate of thickening is rapid and thicknesses greater than 30 nm are reached within 50 h at 300°C. At 250°C, thicknesses of 25–30 nm are obtained after 1000 h exposure. These observations are qualitatively consistent with those of Ringer *et al.* [28] (Fig. 1).

4.2. High resolution electron microscopy

4.2.1. Z-contrast microscopy. Atomic resolution Z-contrast microscopy was used to examine the structure and chemistry of the Ω plate/matrix $(001)_\Omega \parallel (111)_\alpha$ interface in four samples.

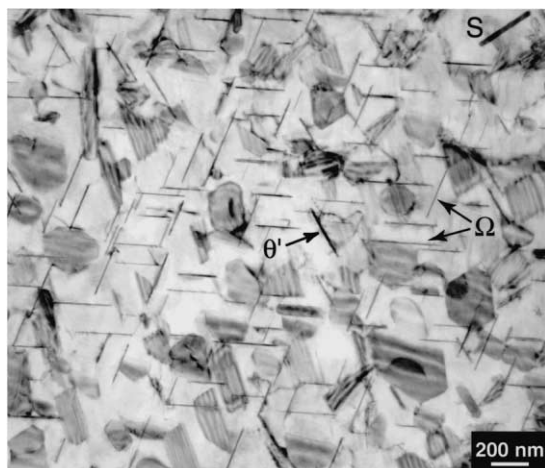


Fig. 4. Bright field TEM micrograph of an Al-4Cu-0.3Mg-0.4Ag (wt. %) alloy. ST 525°C 1 h, WQ, 250°C 10 h. The electron beam is close to $\langle 110 \rangle_\alpha$.

4.2.1.1. Sample 1: 200°C, 100 h. A low magnification Z-contrast image of an Ω plate (right) and a θ' plate (left) is presented in Fig. 5(a). The intensity in a Z-contrast image is approximately proportional to Z^2 and the bright bands bounding each side of the Ω plate are interpreted as preferential segregation of at least Ag to the Ω plate/matrix $(001)_\Omega \parallel (111)_\alpha$ interphase boundary, consistent with previous investigations (Table 1). Ω plates in this orientation [Fig. 5(a)] were found to be very long, straight and typical of Ω plates observed in samples transformed at 200°C. Figure 5(b) is a Z-contrast image of the end of an Ω plate. No such intensity can be seen at the end of the plate. This is interpreted as a lack of significant Ag segregation. Several ledges can be seen (arrowed) on the broad face of the plate. Ledges were rarely observed on plates aged at 200°C for 100 h and those arrowed in Fig. 5(b) represent the only ledges found after analyzing 10–15 plates at this treatment condition. These ledges are $1/2\Omega$ unit cell in height.

An atomic resolution Z-contrast image of a 4 unit

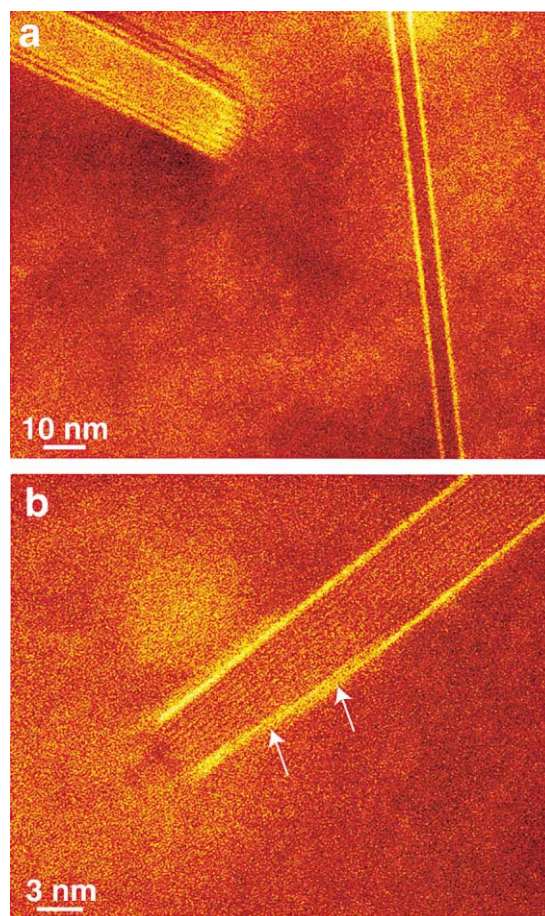


Fig. 5. Low magnification Z-contrast image of Al-4Cu-0.3Mg-0.4Ag (wt. %). ST 525°C 1 h, WQ, 200°C 100 h. The electron beam is close to $\langle 110 \rangle_\alpha$. (a) θ' plate (left) and Ω plate (right) embedded in the Al matrix. (b) end of an Ω plate.

cell thick Ω plate is shown in Fig. 6(a). Two atomic layers of enhanced intensity are seen at the Ω plate/matrix $(001)_{\Omega}|| (111)_{\alpha}$ interface. These correspond to two layers of segregation. This is in contrast to the monoatomic layer reported by Reich *et al.* [38]. The layers of enhanced intensity within the plate parallel to the habit plane are separated by 0.424 nm and correspond to layers enriched in Cu. This is qualitatively consistent with the projection of the proposed orthorhombic Ω structure down zone axes parallel to the habit plane. The Ω phase forms 12 crystallographic variants with the matrix phase. In the $\langle 110 \rangle_{\alpha}$ matrix orientation with a variant of the habit plane parallel to the electron beam, one of the three possible variants will have a $[010]_{\Omega}$ zone axis parallel to the beam, whilst the other two will be indistinguishable and have $\langle 310 \rangle_{\Omega}$ zone axes parallel to the electron beam. It is not possible to determine which variant of Ω is imaged in Fig. 6(a) without clear definition of atomic positions within the Cu and/or Al layers of the plate. Figure 6(b) shows EDS spectra obtained from the matrix, the $(001)_{\Omega}|| (111)_{\alpha}$ interphase boundary and from within the Ω plate. The interfacial segregation was found to contain both Ag and Mg, consistent with most recent analytical investigations (Table 1). A very small Ag peak can be seen in the EDS spectra obtained from both the matrix and from within the Ω plate. The statistical significance of this very small Ag signal is currently being investigated. No obvious enrichment of Mg was detected within the Ω plate or the adjacent matrix. The overall Z-contrast intensity of the Ω plate appears less than the matrix intensity even though the precipitate contains substantial amounts of Cu and the matrix is predominantly Al. The effect is due to preferential thinning of the precipitate during electropolishing. This was confirmed by SEM observations of the foil surface. The reduced volume of the plate material compared with the same matrix cross-section results in a reduced yield of electrons scattered to high angle and captured by the HAADF detector which is used to form the Z-contrast image.

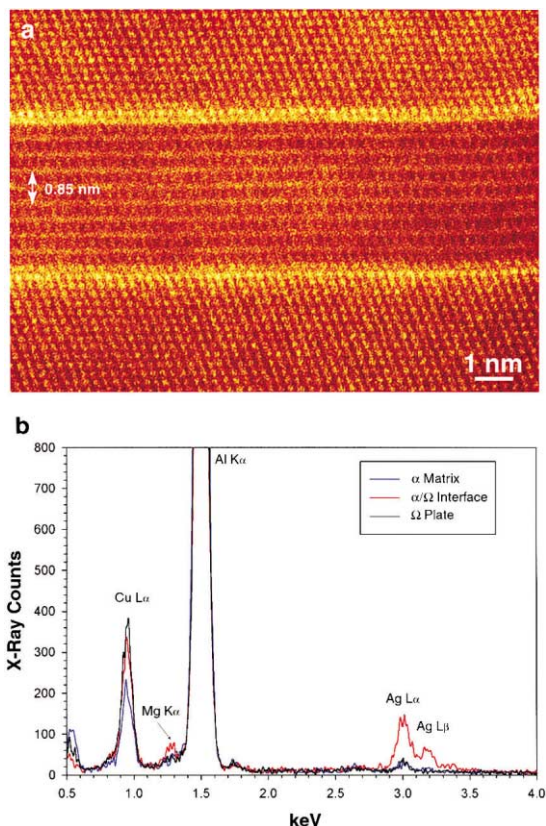


Fig. 6. (a) Atomic resolution Z-contrast image of an Ω plate in Al-4Cu-0.3Mg-0.4Ag (wt. %). ST 525°C 1 h, WQ, 200°C 100 h. The electron beam is close to $\langle 110 \rangle_{\alpha}$. (b) EDS spectra obtained from the adjacent matrix, the $(001)_{\Omega}|| (111)_{\alpha}$ interphase boundary and within the Ω plate.

Fig. 7(a) is a Z-contrast image of an Ω plate thickening ledge in a sample exposed for 70 h at 250°C. The ledge is 1/2 Ω unit cell high and coherent with the matrix. The image shows a double layer of interfacial segregation to the terraces of the thickening ledge. No such inten-

4.2.1.2. *Sample 2: 250°C, 70 h.* Figure 7(a) is a Z-contrast image of an Ω plate thickening ledge in a sample exposed for 70 h at 250°C. The ledge is 1/2 Ω unit cell high and coherent with the matrix. The image shows a double layer of interfacial segregation to the terraces of the thickening ledge. No such inten-

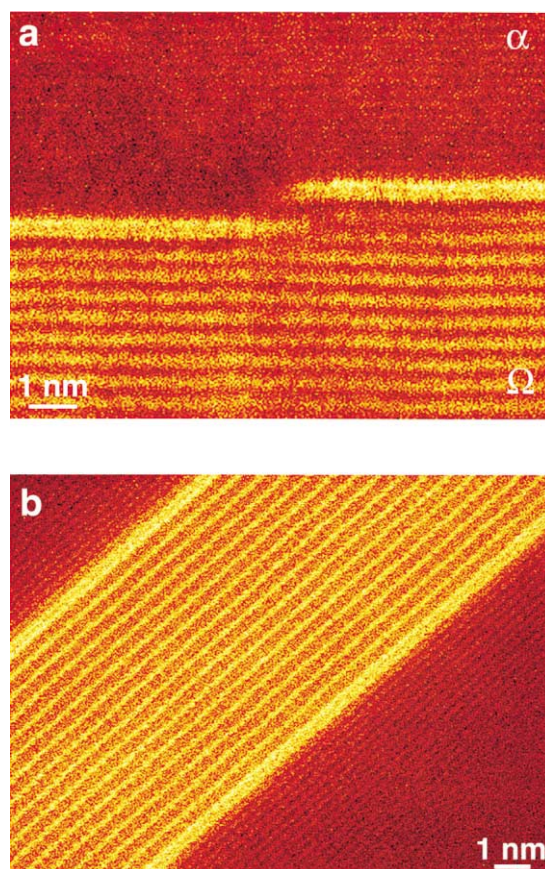


Fig. 7. (a) Z-contrast image of a coherent ledge on an Ω plate in Al-4Cu-0.3Mg-0.4Ag (wt. %). ST 525°C 1 h, WQ, 250°C 70 h. The electron beam is close to $\langle 112 \rangle_{\alpha}$. (b) Atomic resolution Z-contrast image of an Ω plate in Al-4Cu-0.3Mg-0.4Ag (wt. %). ST 525°C 1 h, WQ, 250°C 475 h. The electron beam is close to $\langle 110 \rangle_{\alpha}$.

sity can be seen at the riser of the ledge. This is interpreted as a lack of Ag segregation to the riser of the ledge, consistent with the APFIM observations of Reich *et al.* [38]. The presence of Mg in the vicinity of the ledge riser cannot be determined on the basis of intensity in the Z-contrast images. The atomic positions in the Al matrix are not resolved in this micrograph since their separation in this orientation is beyond the resolution of the VG HB603U microscope. Energy dispersive spectra were obtained from the matrix, the $(001)_{\Omega}|| (111)_{\alpha}$ interphase boundary and wholly within the Ω plate. They showed segregation of both Ag and Mg to the interface. As was the case for the sample treated at 200°C, a very small Ag peak was found in the EDS spectra collected both from within the Ω plate and the adjacent matrix. No obvious enrichment of Mg was detected within the Ω plate or the matrix.

4.2.1.3. Sample 3: 250°C, 475 h. The atomic resolution Z-contrast image in Fig. 7(b) again shows a double layer of interfacial segregation under this treatment condition. The EDS analysis found the segregation to consist of both Ag and Mg. Again, a very small Ag peak was found in the EDS spectra collected both from within the Ω plate and the adjacent matrix. No obvious enrichment of Mg was detected within the Ω plate or the matrix.

4.2.1.4. Sample 4: 300°C, 50 h. At 300°C the Ω plates thickened at a greatly enhanced rate, and the Z-contrast image in Fig. 8 shows thickening ledges are plentiful on the Ω plate. Two atomic layers of segregation to the Ω plate/matrix $(001)_{\Omega}|| (111)_{\alpha}$ interface were again observed. EDS confirmed that the intensity seen at the plate/matrix interface in the Z-contrast image was due to both Ag and Mg segregation. Again, a very small Ag peak was detected in the EDS spectra collected both from within the plate and the adjacent matrix. No obvious enrichment of Mg was detected

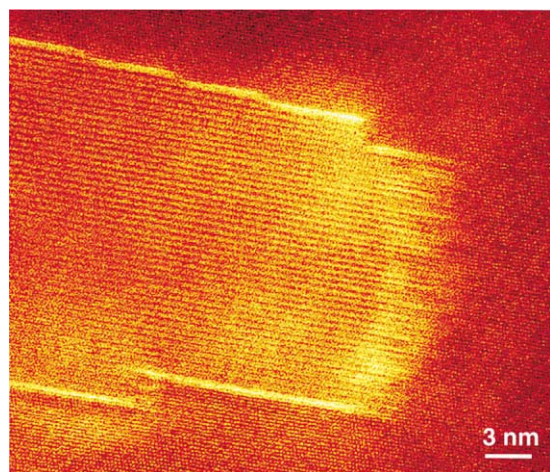


Fig. 8. High magnification Z-contrast image of the end of a thick Ω plate in Al-4Cu-0.3Mg-0.4Ag (wt. %). ST 525°C 1 h, WQ, 300°C 50 h. The electron beam is close to $\langle 110 \rangle_{\alpha}$.

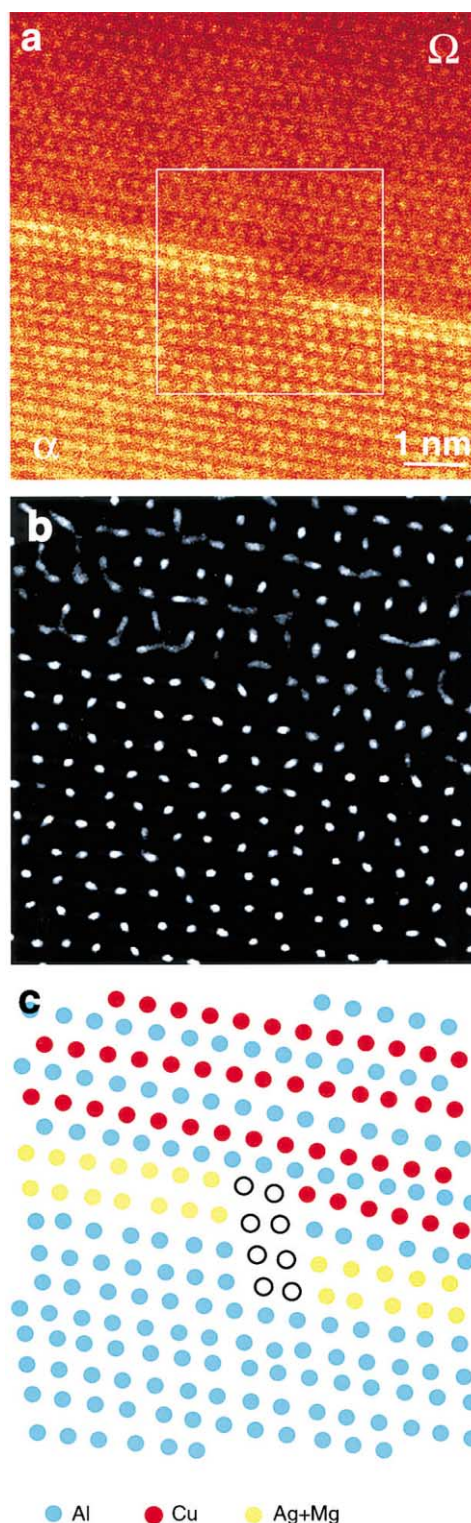
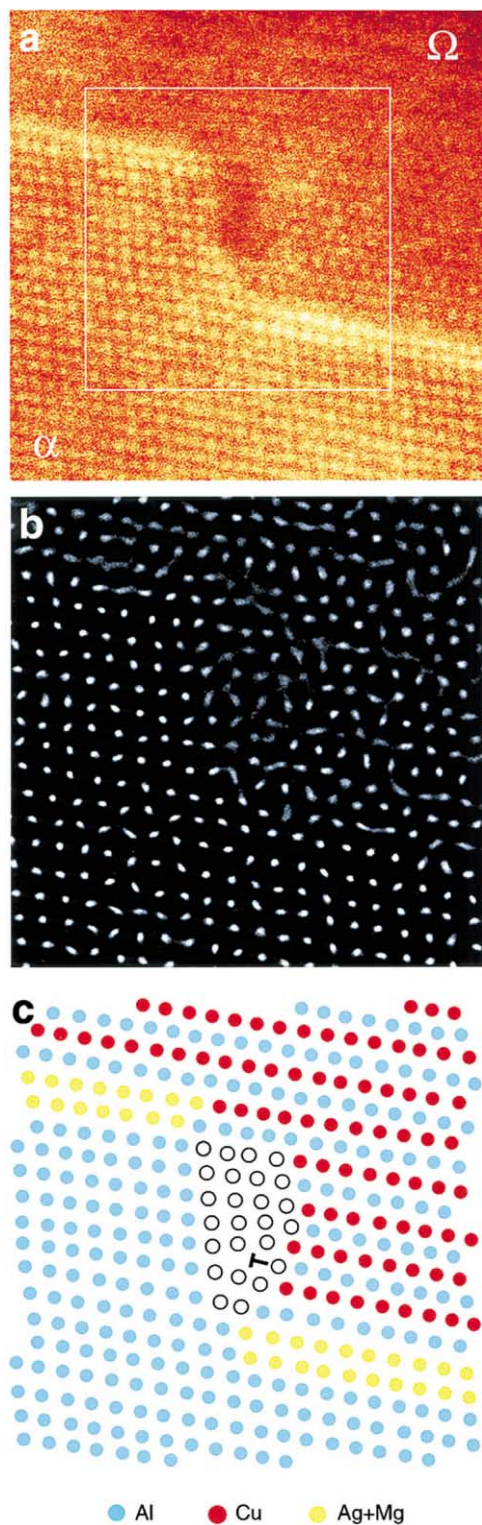


Fig. 9. (a) Atomic resolution Z-contrast image of a $1/2$ Ω unit cell high coherent thickening ledge on an Ω plate in Al-4Cu-0.3Mg-0.4Ag (wt. %). ST 525°C 1 h, WQ, 300°C 50 h. The electron beam is close to $\langle 110 \rangle_{\alpha}$. (b) Entropy maximized image of inset in (a). (c) Schematic model of (b) illustrating the atomic arrangement of species in the vicinity of the ledge. Open circles correspond to well defined atomic positions but the identity of the species is unclear from the Z-contrast image.

within the Ω plate or the matrix. A rim of intensity is seen at the end of the plate in Fig. 8. This was examined using EDS and it is concluded that the intensity is not associated with Ag segregation or an excess of Cu. The rim of intensity is a result of the change in foil thickness associated with the etching of the Ω



phase during electropolishing. The Cu content of the Ω plate is nominally constant along the length of the plate but an increase in foil thickness associated with the end of the plate results in an increase in the yield of electrons scattered to high angles and captured by the HAADF detector. Different sized ledges can be observed on the broad faces of the Ω plate shown in Fig. 8. Small $1/2$ Ω unit cell high ledges are observed on the top face of the plate, whilst a much larger ledge can be seen on the lower broad face. These ledges are examined in detail in Figs 9 and 10 and are consistent with the two types of ledges observed by Fonda *et al.* [37] in their studies of misfit strain accommodation surrounding Ω plates. The smaller $1/2$ Ω unit cell ledge shown in Fig. 9(a) is fully coherent with the matrix. Nucleation of the ledge replaces two matrix $\{111\}_\alpha$ planes. The lower overall intensity of the Ω plate in comparison with the matrix in the Z-contrast image is again due to preferential thinning of the Ω plate during electropolishing. Figure 9(b) is an entropy maximized image of (a), and (c) is a schematic illustration of the atomic arrangement around the coherent ledge. The Cu columns in the Ω phase are clear, as is the Ag and Mg segregation to the interface. The well defined positions of the Cu columns allows the orientation of the plate with respect to the electron beam to be determined as the $[010]_\Omega$ orientation. The open circles represent well defined atomic positions but the identity of the species is unclear from the intensity in the Z-contrast image. Figure 9 illustrates that an Al layer in the Ω phase is immediately adjacent to the layers of Ag and Mg segregation. This is clearly represented in the schematic of Fig. 9(c). Figure 10(a) is a Z-contrast image of a larger ledge found on the same plate imaged in Fig. 9. The layers of interfacial segregation are again seen but a dark patch of intensity is observed near the riser of the ledge. The atomic positions in the vicinity of the ledge were determined from the entropy maximized image in (b) and a schematic illustration of the atomic arrangement can be seen in (c). The ledge is $2\ 1/2$ Ω unit cells high and is not coherent with the matrix. The ledge contains a misfit compensating dislocation. It appears as a Frank partial dislocation ($b = 1/3[111]_\alpha$) with the extra half-plane in the precipitate phase. Some discrepancies exist between the Z-contrast images in Figs 9 and 10 and the images expected from the orthorhombic model for the Ω unit cell. These discrepancies concern the positions of the Al atoms within the cell and suggests further work is needed in this area.

Fig. 10. (a) Atomic resolution Z-contrast image of a $2\ 1/2$ Ω unit cell high thickening ledge on an Ω plate in Al-4Cu-0.3Mg-0.4Ag (wt. %). ST 525°C 1 h, WQ, 300°C 50 h. The electron beam is close to $\langle 110 \rangle_\alpha$. (b) Entropy maximized image of inset in (a). (c) Schematic model of (b) illustrating the atomic arrangement of species in the vicinity of the ledge. Open circles correspond to well defined atomic positions but the identity of the species is unclear from the Z-contrast image. The ledge is not coherent with the matrix. A dislocation of the type $1/3\langle 111 \rangle_\alpha$ can be seen with the extra half-plane in the precipitate phase.

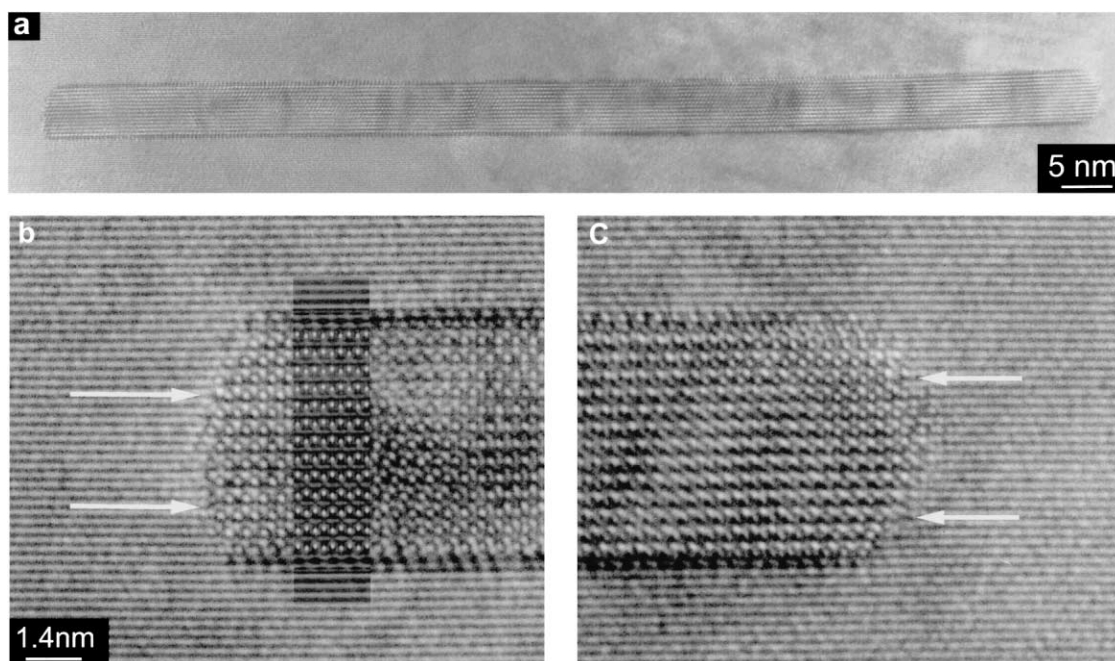


Fig. 11. (a) High resolution phase contrast image of an Ω plate after exposure for 1000 h at 200°C. The plate contains no ledges. $\mathbf{B} = \langle 112 \rangle_{\alpha} \parallel [110]_{\Omega}$ (b) High magnification image of the left end of the plate in (a). The plate is 6.5 Ω cells thick. The end of the plate contains two dislocations (arrowed) of type $1/3 \langle 111 \rangle_{\alpha}$ with the extra half plane in the precipitate phase. A high resolution simulation is included as an inset (-70 nm defocus, 11 nm foil thickness). (c) High magnification view of the right end of the plate showing dislocations.

4.2.2. High resolution phase contrast microscopy.

The Z-contrast observations indicated thickening ledges were rarely observed on Ω plates treated at 200°C. Conventional high resolution phase contrast imaging has been used to examine the generality of this observation in samples treated for 10 and 1000 h at 200°C.

In almost all cases the plates observed did not contain any ledges. A typical example is shown in Fig. 11(a). Ten Ω plates have been documented from HRES images and the ledge density and thickness of each of the plates recorded in Table 2. Of the ten plates recorded on film, only one plate contained a ledge. The ledges observed in Fig. 5(b), Fig. 7(a), on

the top face in Fig. 8, and in Fig. 9 were all $1/2 \Omega$ unit cell in height and coherent with the matrix. A survey of the literature also shows that when ledges are observed on Ω plates, they are most commonly $1/2 \Omega$ unit cell in height [26, 37]. Fonda *et al.* [37] showed that the nucleation of a $1/2 \Omega$ unit cell coherent ledge ($(1/2)[001]_{\Omega} = 0.424$ nm) replaces two matrix $(111)_{\alpha}$ planes ($2/3[111]_{\alpha} = 0.4676$ nm) and produces an additional vacancy misfit (Fig. 2) normal to the plate of more than 0.04 nm, and that this misfit is sufficient to substantially alter the strain field surrounding a precipitate plate. Fonda *et al.* [37] used the anomalous Ashby-Brown contrast [48, 49] to show that the Ω plates observed in that study always

Table 2. Summary of Ω plate thickness and ledge density recorded from high resolution phase contrast images of samples treated at 200°C

Ω Plate	Heat treatment condition	Plate thickness (Ω unit cells)	Number of coherent $1/2 \Omega$ unit cell high ledges	Inferred number of $1/3 \langle 111 \rangle_{\alpha}$ dislocations at plate ends	Unrelaxed misfit* (%) in $[001]_{\Omega} \parallel [111]_{\alpha}$ direction
1	200°C, 10 h	4	0	1	-24.6
2	200°C, 10 h	1	0	0	-18.7
3	200°C, 10 h	2.5-3.5	2 ^b	1	+3.38 -15.3
4	200°C, 10 h	2.5	0	1	+3.38
5	200°C, 10 h	3	0	1	-5.9
6	200°C, 1000 h	6	0	2	-11.9
7	200°C, 1000 h	6	0	2	-11.9
8	200°C, 1000 h	7	0	2	-30.5
9	200°C, 1000 h	6.5	0	2	-21.2
10	200°C, 1000 h	5.5	0	2	-2.6

* Unrelaxed misfit (%) = (unrelaxed misfit (nm) (Fig. 12)) / ($2/3[111]_{\alpha} = 0.4676$ nm) * 100.

^b The ledge on this plate is in fact a single 1Ω unit cell high coherent ledge.

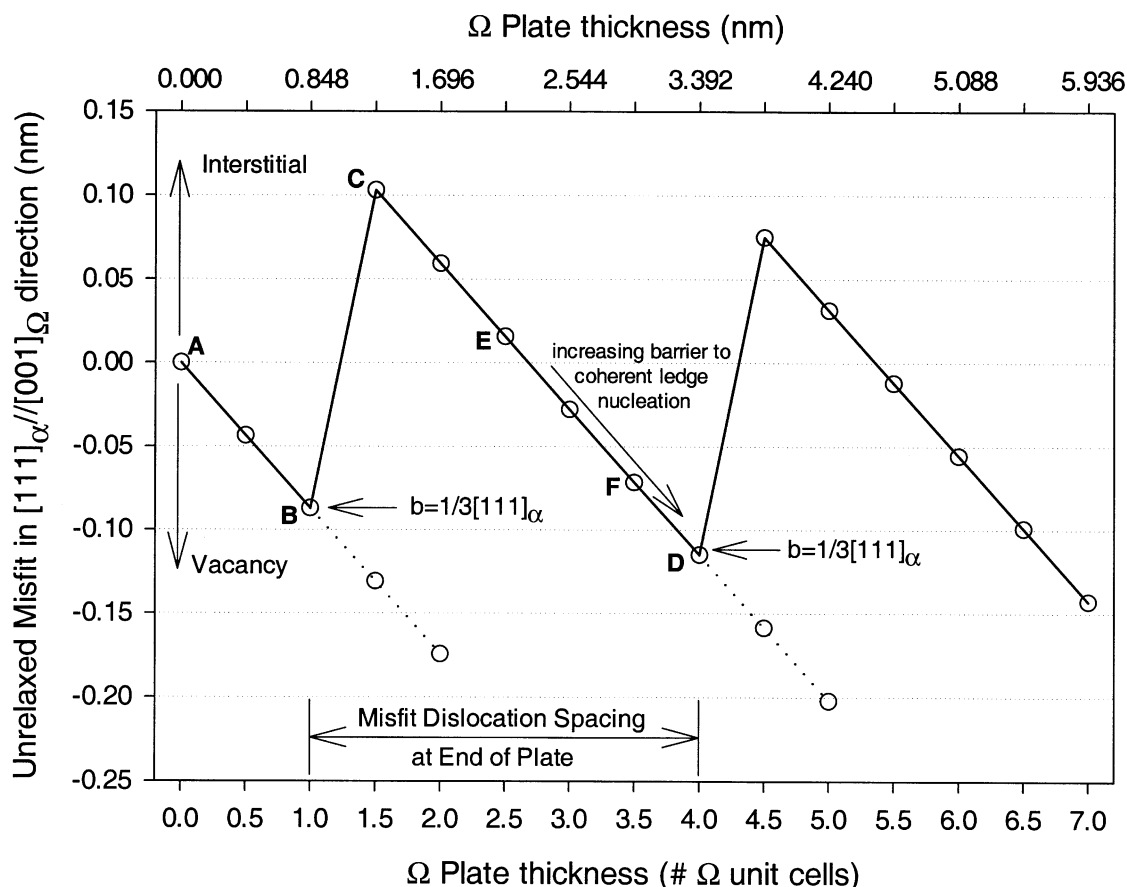


Fig. 12. Plot of the change in unrelaxed misfit (nm) normal to the Ω plate habit plane as a function of Ω plate thickness.

displayed a vacancy type misfit field regardless of plate thickness. The plates were formed at the relatively high temperature of 375°C giving rise to a coarse distribution. The distributions of plates observed at 200°C is very fine and overlapping strain fields precludes the unambiguous interpretation of the anomalous Ashby-Brown contrast to determine the residual misfit of the plates. However, plate thicknesses can be determined directly from HRES images and this has been illustrated in Fig. 11(b). The interpretation of high resolution phase contrast from interfaces can be very difficult without prior knowledge of the structure of the interface [50]. In this case the geometry of the interface is known from the incoherently formed Z-contrast images in Figs 9 and 10. The number of segregation layers and the nature of the layer in the precipitate phase adjacent to the segregation are each known. A high resolution simulation was performed from a model structure containing a 6.5 Ω unit cell thick plate bounded by two atomic layers of mixed Ag and Mg and embedded in the Al matrix. The simulation inset is shown in Fig. 11(b). The agreement between experimental and simulated images is satisfactory and it is concluded that the plate is 6.5 Ω unit cells in thickness. The thickness of each of the 10 plates examined has been evaluated

and included in Table 2. This information along with the number of Frank partial dislocations at the ends of the plates allows the unrelaxed misfit normal to the plate to be calculated. The plate shown in Fig. 11 corresponds to plate 9 in Table 2. This plate is suitably oriented to directly image the Frank partial dislocations at the ends of the plate. Figure 11(b,c) are enlarged images of both ends of the plate in (a). Two misfit dislocations exist at the end of this 6.5 unit cell thick plate and have been clearly labeled.

5. DISCUSSION

5.1. The role of ledge nucleation/migration in the coarsening resistance of Ω plates

This study has shown that despite considerable differences in Ω plate thickening kinetics between 200 and 300°C, no significant changes in the segregation behavior of Ag and Mg are observed. Two atomic layers of Ag and Mg segregation are found at the coherent broad faces of the plates. No Ag segregation is found at the risers of thickening ledges, consistent with the observations of Reich *et al.* [38], nor is any Ag segregation observed at the ends of the plates. Only very small quantities of Ag and Mg (if any at

all) were detected within the plates themselves. Consequently, the necessary Ag and Mg redistribution from the broad face of the plate to the terrace of a migrating ledge (Fig. 3) must be accompanying ledge migration at all temperatures. Any interaction between the redistributing Ag and Mg and the flux of Cu to the ledge riser (Section 2.3) is expected to occur at all temperatures and is not considered unique to temperatures below 200°C. Therefore, if an interaction does exist it is not considered to play the decisive role in the excellent coarsening resistance exhibited by Ω plates at temperatures up to 200°C. The characteristic feature that distinguishes Ω plates transformed at 200°C from those at higher temperatures is the thickening ledge density. Samples transformed at 200°C for times greater than 10 h rarely contained ledges (Table 2). A large increase in thickening ledge density was observed for samples treated at 300°C (Fig. 8), concomitant with greatly enhanced plate thickening kinetics. The excellent coarsening resistance of Ω plates at temperatures up to 200°C can be ascribed to a limited supply of thickening ledges. The most commonly observed thickening ledges on Ω plates are coherent and $1/2 \Omega$ unit cell in height. Nucleation of these ledges replaces two matrix $\{111\}_\alpha$ planes and introduces a vacancy misfit of more than 0.04 nm normal to the habit plane of the plate [37]. The nucleation of a coherent misfitting crystal in an elastically constrained matrix can be strongly influenced by elastic interactions with pre-existing strain fields in the matrix [51]. A particularly illustrative example is the heterogeneous nucleation of δ' (Al_3Li) precipitates in the strain field of edge dislocations in dilute Al–Li alloys [52, 53]. A pure dilatational (vacancy) strain field is associated with the formation of spherical coherent δ' precipitates. Cassada *et al.* [52] demonstrated that at small undercoolings the most favorable nucleation site for these precipitates is the compressive side of edge dislocations since the strain field of the dislocation mitigates the dilatational field of the δ' precipitate. An analogy can be drawn between the heterogeneous nucleation of coherent misfitting thickening ledges on Ω plates and the nucleation of δ' precipitates on dislocations. Since the $1/2 \Omega$ unit cell high coherent ledge exhibits a vacancy misfit normal to the plate, on the basis of volumetric misfit alone, the nucleation probability would be highest (activation barrier is lowest) when the plates exhibit a residual interstitial misfit and increasingly less probable for increasing vacancy strains normal to the broad face of the plate. A plot of the change in unrelaxed misfit (expressed in nm) normal to the Ω plate habit plane as a function of Ω plate thickness is shown in Fig. 12. This figure was constructed with the aid of several experimental observations. Single unit cell thick Ω precipitates are known to be fully coherent with the Al matrix ([26] and (Table 2, plate 2). The average spacing of Frank partial dislocations at the ends of relatively thick plates is 2.5 or 3Ω unit cells [37], and a 6.5 unit cell

thick precipitate contains 2 Frank partial dislocations (Fig. 11). As successive coherent vacancy misfitting $1/2 \Omega$ unit cell ledges are added to the broad face of a plate, the overall vacancy misfit normal to the plate increases. This is represented by the solid line (AB) in Fig. 12. Above some critical value of this misfit† it becomes energetically favorable for a dislocation of the type $\mathbf{b} = 1/3[111]_\alpha$ to form with the extra half plane in the precipitate phase [e.g. Fig. 11(b)]. The resulting misfit becomes interstitial in nature ($B \rightarrow C$, Fig. 12). Subsequent nucleation of coherent vacancy misfitting ledges relaxes the interstitial misfit and the strain field normal to the broad face once again becomes vacancy in nature ($C \rightarrow D$, Fig. 12) with a concomitant increase in the activation barrier for coherent vacancy misfitting ledge nucleation. For those plates transformed at 200°C and listed in Table 2, the inferred number of Frank partial dislocations and the unrelaxed misfit normal to the plate have been evaluated on the basis of Fig. 12. The table shows that in all cases except plates 3 and 4, a vacancy misfit exists normal to the plate. In the case of plate 4, the misfit is interstitial, albeit only slightly. These plates contain no ledges because the nucleation barrier for a coherent vacancy misfitting ledge in a pre-existing vacancy field is prohibitively large. Plate 3 provides an interesting example. It was the only plate observed with a ledge, and the ledge is a single coherent full Ω unit cell in height. The plate was initially 2.5 cells thick, corresponding to an interstitial strain field (E , Fig. 12) but after propagation of the ledge, the plate is 3.5 cells thick with a strong vacancy misfit (F , Fig. 12). Nucleation of the coherent vacancy misfitting ledge is assisted through mitigation of the interstitial strain field normal to the plate. Some examples from the literature can also be used to show that plate thicknesses and ledge densities can be rationalized on the basis of Fig. 12. Rarely, are high resolution images of an entire Ω plate included in the literature. This means a rationalization can only be attempted for those images of plates that do contain ledges. Figure 7(a) in the paper of Garg *et al.* is an Ω plate containing two $1/2 \Omega$ unit cell high ledges. One end of the plate is 7.5 Ω cells thick and the other 8.5 Ω cells thick. A plate 7.5 cells thick will contain three Frank partial dislocations at its end and will be strongly interstitial in misfit (Fig. 12). These are very favorable conditions for the nucleation of coherent vacancy misfitting ledges. Figure 16 in the same paper shows a two unit cell thick plate containing a single $1/2 \Omega$ unit cell ledge. A two unit cell thick plate contains a single Frank partial at the end of the

† The critical misfit normal to the plate corresponding with the formation of a Frank partial dislocation of the type $\mathbf{b} = 1/3[111]_\alpha$ may depend on plate thickness. At very small plate thicknesses, the plate is expected to behave as an elastically constrained thin film, but as the plate thickens the elastic properties of the plate would be expected to more closely approach those of bulk Ω .

plate and is strongly interstitial in misfit, again conditions are favorable for the nucleation of coherent vacancy misfitting ledges.

In all cases observed, plates that contain ledges have a residual interstitial misfit (or only slightly vacancy) and those that contain no ledges exhibit a vacancy misfit[†]. Most of the plates listed in Table 2 exhibit strong vacancy misfits, conditions very unfavorable for the nucleation of coherent vacancy misfitting ledges. It has been possible to rationalize the plate thicknesses and ledge densities encountered in this study on the basis of volumetric misfit alone. It is concluded that nucleation of coherent ledges during the coarsening stages of Ω plate thickening are dominated by strain energy considerations and that this effect is responsible for the excellent coarsening resistance of Ω plates at temperatures up to 200°C. The free energy change attending the homogeneous nucleation of a coherent ledge on the broad face of a plate-like precipitate has been reported by Weatherly [54, 55]. However, in most subsequent derivations of the activation barrier for ledge nucleation, the contribution from elastic interactions between the nucleus and a pre-existing strain field are ignored [54–56]. For ledge nucleation during the coarsening stages of Ω plates, this contribution has an integral role and further work is required on the mathematical representation of this interaction for explicit incorporation into classical nucleation theory.

The analysis presented above applies only at relatively small plate thicknesses. The matrix dislocation density greatly increased during the later stages of thickening of Ω plates at 250 and 300°C and these dislocations interacted strongly with both the edges and the broad faces of the plates, presumably to aid in the accommodation of strain associated with the plate. The regime of thickening that includes the generation of matrix dislocations and their interaction with the strain fields of the plates is beyond the scope of this study.

5.2. Implications of Ag and Mg segregation in the stability of a uniform distribution of Ω plates

It is well documented that trace additions of Ag and Mg to Al–Cu alloys greatly facilitates the nucleation of the Ω phase [3–6]. Ag and Mg segregation was found, without exception, to the broad faces of the Ω plates at all times and temperatures observed regardless of plate aspect ratio. This is interpreted to mean that this segregation is also a phenomenon associated with growth and coarsening pro-

cesses and is necessary for stability of the Ω plate on the $\{111\}_\alpha$ planes of the matrix in this alloy. Despite a report that Ω can form in the ternary Al–Cu–Mg system [57] (i.e. in the absence of Ag), no cases of $\{111\}_\alpha$ plates forming without Ag and Mg segregation or with only partial segregation to the broad faces were observed in the present study. Furthermore, the Ω plates were not observed to outlengthen their layers of Ag and Mg segregation, at any stage [e.g. Fig. 5(b)] despite the comparatively high interface mobility of the ends of the plates. Lengthening of the Ω plate must involve the long range diffusion of Cu, Ag and Mg from the matrix. The Ag and Mg is necessary to stabilize the newly formed $(001)_\Omega \parallel (111)_\alpha$ interface upon plate lengthening. This is to be contrasted with the thickening of Ω plates that involves only the long range diffusion of Cu from the matrix and a *redistribution* of Ag and Mg around the thickening ledge. The lengthening of Ω plates can be restricted either by a limited supply of Cu or a limited supply of Ag and Mg in the matrix. The co-clustering of Ag and Mg that precedes the formation of Ω plates [38] gives rise to a non-uniform distribution of Ag and Mg in the matrix. Only very small quantities of Ag and Mg (if any at all) were detected within the matrix using EDS during this study. It is likely that soon after the development of a fine dispersion of Ω plates most of the Ag and Mg is associated with Ω plates or other Mg containing phases such as equilibrium S (Al_2CuMg). This is fortuitous for alloy designs based on Ω as a finely distributed thermally stable phase. The tendency for Ω plates to form with highly non-equilibrium aspect ratios, as observed with $\gamma'(\gamma)$ in Al–Ag alloys [58–60], will be reduced in Al–Cu–Mg–Ag alloys because of the unavailability of additional Ag and Mg and the associated internal restriction for lengthening. The restriction on lengthening also means that the frequency of plate impingement must be reduced. Sites of plate impingement are reported to be very potent ledge nucleation sites for θ' in Al–Cu alloys [31] and $\gamma'(\gamma)$ in Al–Ag alloys [61]. The frequency of ledges nucleated in this way will be reduced in these alloys. This is important considering the decisive role ledge nucleation plays in the coarsening resistance of the Ω plates (Section 5.1).

5.3. Accommodation of the misfit normal to an Ω plate as a possible reason for Ag and Mg segregation?

The segregation of Ag and Mg to the broad face of the Ω plate occurs because it lowers the total free energy of the system. This does not necessarily imply a lowering of the interfacial energy of the $(001)_\Omega \parallel (111)_\alpha$ interface. It has been proposed that the segregation may occur to aid in accommodation of the large misfit that exists between Ω and the Al lattice, normal to the habit plane [15, 17, 23, 69]. The reported misfit of -9.3% is evaluated on the basis of lattice parameter misfit alone. As shown in Section 5.1, the misfit normal to a precipitate plate

[†] Fonda *et al.* [37] observed that the average spacing of Frank partial dislocations at the ends of thick plates was 2.5–3.0 Ω unit cells. This is an *average* spacing and was used to construct Fig. 12. Deviations from this average spacing may reveal plate thicknesses that appear inconsistent with the arguments presented above on the basis of Fig. 12. In those cases, direct observation of the number of dislocations at the ends of the plates is necessary.

is not constant and will depend critically on both the thickness of the precipitate plate and the mechanisms of strain accommodation existing normal to the plate. In this study, two atomic layers of Ag and Mg segregation was observed at all times and temperatures, regardless of plate thickness. Table 2 shows that plates exist with a variety of residual misfits (both vacancy and interstitial). If the primary purpose of Ag and Mg segregation is to help accommodate the misfit normal to the plate then a variety in the number of layers of segregation (and possibly the Ag:Mg ratio within the layers) would also be expected. This would help accommodate the spectrum of misfits associated with a variety of plate thicknesses. This is strikingly illustrated in Fig. 7(a) and Fig. 9 which show coherent $1/2 \Omega$ unit cell high ledges. Nucleation of these ledges contributes an additional -9% misfit to the pre-existing strain field normal to the plate. Since the ledge is coherent with the matrix, there are no other mechanisms (except for local elastic relaxations) that may be operating to reduce the misfit. Despite a difference in residual strain of more than 9% normal to the plate, both the habit plane and the terrace of the migrating ledge contain two atomic layers of segregation. Furthermore, the rationalization of plate thickness and ledge nucleation kinetics on the basis of the strain normal to the plate (Section 5.1), was made assuming the presence of Ag and Mg did not have a significant effect on the misfit normal to the plate. If the Ag and Mg did have a significant effect on the accommodation of strain normal to the plate, then some plates would be expected to be stabilized at thicknesses that would correspond to interstitial residual strains according to Fig. 12. This was not the case, and Fig. 12 was able to adequately describe the experimental observations. Recent 3D-APFIM results have also shown that Ag and Mg segregate to the broad faces of T_1 plates in Al-Cu-Mg-Li-Ag alloys [64]. These plates have a very small misfit (0.12%) normal to the plate, and accommodation of this very small misfit as a driving force for Ag and Mg segregation seems unlikely. It is therefore concluded that the primary reason for Ag and Mg segregation is not to accommodate the reportedly high misfit normal to the Ω plates. Nie *et al.* [62] and Muddle and Nie [63] have already expressed doubts concerning the accommodation of the volumetric strain normal to the Ω plate as a driving force for Ag and Mg segregation. Their arguments were based on the catalyzing effect Ag and Mg has on the nucleation of both Ω and T_1 plates.

On the basis of a lattice correspondence analysis, Nie *et al.* [62] and Muddle and Nie [63] have recently suggested that the transformation strain associated with the formation of plate-shaped precipitates such as Ω can often have a significant shear component. They suggest the accommodation of shear strain energy is an important factor controlling both nucleation and growth. The rationalization of plate

thicknesses and ledge densities in Section 5.1 was made on the basis of volumetric misfit alone. The misfit associated with the shape change attending the nucleation of coherent misfitting ledges on the broad face of the Ω plate was not incorporated. That this approach was successful does not necessarily imply that the strain associated with the shape change is not important, rather, it may suggest that some mechanism is operating to accommodate the shape strain. In light of these results, the accommodation of the shear component of the transformation strain may also be an important factor in attempts to identify the energetics of Ag and Mg segregation to the broad faces of these plates.

6. CONCLUSIONS

1. At all temperatures examined the thickening of Ω plates shows a linear dependence on time. At 200°C , Ω plates reach thicknesses of approximately 5.5 nm after 100 h exposure, after which there is no detectable change in the average thickness. The plate thickening rate increased at 250°C with thicknesses of $25\text{--}30 \text{ nm}$ being reached after 1000 h exposure. Further increases in plate thickening kinetics occurs at 300°C , with thickness in excess of 30 nm reached within 50 h . These observations are qualitatively consistent with the observations of Ringer *et al.* [28].
2. Z-contrast observations revealed two atomic layers of Ag and Mg segregation to the $(001)_\Omega \parallel (111)_\alpha$ interphase boundary at all times and temperatures examined. No segregation of Ag was found to the risers of thickening ledges or to the ends of the plates. Only very small quantities of Ag and Mg (if any at all) were detected within the plate at any time.
3. The necessary Ag and Mg redistribution from the broad face of the plate to the terrace of the migrating thickening ledge must accompany ledge migration at all temperatures. The Ag and Mg redistribution is not considered to play a decisive role in accounting for the excellent coarsening resistance of Ω plates at temperatures up to 200°C .
4. Consistent with previous investigations of the thickening kinetics of precipitate plates in Al-alloys [30–32], the thickening of Ω plates is restricted by a limited supply of ledges. The density of thickening ledges on plates transformed for times longer than 10 h at 200°C was very low, usually zero. A large increase in ledge density is associated with the increase in thickening kinetics at 250 and 300°C .
5. The prohibitively high barrier to coherent ledge nucleation on the broad faces of plates aged at 200°C is due to the contribution to the total free energy change attending nucleation from elastic interactions between the misfitting coherent ledges

and the significant strain field that can exist normal to the broad face of the Ω plate.

6. Accommodation of the large misfit that exists normal to the broad face of the Ω plate is unlikely to provide the driving force for Ag and Mg segregation. Since two layers of Ag and Mg segregation were observed to the broad faces of plates of various thicknesses (and therefore various misfits), another explanation seems likely.

Acknowledgements—CRH and GJS greatly acknowledge the support of the Southeastern Universities Research Association 1999 Summer Cooperative Research Program and the National Science Foundation under grant number DMR-9904034. The work at Oak Ridge National Laboratory was supported by the Division of Materials Sciences, US Department of Energy under contract No. DE-AC05-00OR22725 with UT-Battelle, LLC. Dr Simon Ringer of the Electron Microscopy Unit at the University of Sydney, Australia is thanked for kind provision of materials used in this study.

REFERENCES

- Polmear, I. J., *Nature*, 1960, **186**, 303.
- Polmear, I. J., *Trans. Metall. Soc. AIME*, 1964, **230**, 1331.
- Auld, J. H. and Vietz, J. T., in *The Mechanism of Phase Transformations in Crystalline Solids, Monograph and Report Series, No. 33*. Institute of Metals, London, 1969, p. 77.
- Taylor, J. A., Parker, B. A. and Polmear, I. J., *Metals Sci.*, 1978, **12**, 478.
- Chester, R. J. and Polmear, I. J., *Micron*, 1980, **11**, 311.
- Chester, R. J. and Polmear, I. J., in *The Metallurgy of Light Alloys*. Institute of Metals, London, 1983, p. 75.
- Polmear, I. J. and Couper, M. J., *Metall. Trans.*, 1988, **19A**, 1027.
- US Patent #3,414,406, Patented Dec. 3, 1968.
- US Patent #4,610,733, Patented Sept. 9, 1986.
- Polmear, I. J., Pons, G., Barbaux, Y., Octor, H., Sanchez, C., Morton, A. J., Borbidge, W. E. and Rogers, S., *Mater. Sci. Tech.*, 1999, **15**, 861.
- Auld, J. H., *Acta crystallogr.*, 1972, **A28**, S98 Suppl.
- Auld, J. H., *Mater. Sci. Technol.*, 1986, **2**, 784.
- Kerry, S. and Scott, V. D., *Metal Sci.*, 1984, **18**, 289.
- Scott, V. D., Kerry, S. and Trumper, R. L., *Mater. Sci. Technol.*, 1987, **3**, 827.
- Garg, A. and Howe, J. M., *Acta metall.*, 1991, **39**, 1939.
- Knowles, K. M. and Stobbs, W. M., *Acta crystallogr.*, 1988, **B44**, 207.
- Muddle, B. C. and Polmear, I. J., *Acta metall.*, 1989, **37**, 777.
- Vaughan, D. and Silcock, J. M., *Physica status solidi*, 1967, **20**, 725.
- Abis, S., Mengucci, P. and Riontino, G., *Phil. Mag. B*, 1993, **67**, 465.
- Cousland, S. McK. and Tate, G. R., *J. Appl. crystallogr.*, 1986, **19**, 174.
- Lim, M. S., Tibballs, J. E. and Rossitter, P. L., *Z. Metallk.*, 1997, **88**, 236.
- Garg, A. and Howe, J. M., *Acta metall. mater.*, 1991, **39**, 1925.
- Ringer, S. P., Hono, K., Polmear, I. J. and Sakurai, T., *Acta metall. mater.*, 1996, **44**, 1883.
- Hono, K., Sakurai, T. and Polmear, I. J., *Scripta metall.*, 1994, **30**, 695.
- Suh, I. S. and Park, J. K., *Scripta metall.*, 1995, **33**, 205.
- Garg, A., Chang, Y. C. and Howe, J. M., *Acta metall. mater.*, 1993, **41**, 235.
- Chang, Y. C. and Howe, J. M., *Metall. Trans. A*, 1993, **24A**, 1461.
- Ringer, S. P., Yeung, W., Muddle, B. C. and Polmear, I. J., *Acta metall. mater.*, 1994, **42**, 1715.
- Aaronson, H. I., in *Decomposition of Austenite by Diffusional Processes*, ed. V. F. Zackay and H. I. Aaronson. Interscience, New York, 1962, p. 387.
- Aaronson, H. I. and Laird, C., *Trans. AIME*, 1968, **242**, 1437.
- Sankaran, R. and Laird, C., *Acta metall.*, 1974, **22**, 957.
- Laird, C. and Aaronson, H. I., *Acta metall.*, 1969, **17**, 505.
- Sankaran, R. and Laird, C., *Scripta metall.*, 1977, **11**, 383.
- Aaronson, H. I., Lee, J. K. and Russell, K. C., in *Proceedings of a symposium sponsored by the TMS-AIME Heat Treatment Committee at the 1976 TMS Fall Meeting*, Niagara Falls, New York, 1976, p. 31.
- Stobbs, W. M. and Purdy, G. R., *Acta metall.*, 1978, **26**, 1069.
- Dahmen, U. and Westmacott, K. H., *Physica status solidi*, 1983, **80(A)**, 249.
- Fonda, R. W., Cassada, W. A. and Shiflet, G. J., *Acta metall. mater.*, 1992, **40**, 2539.
- Reich, L., Murayama, M. and Hono, K., *Acta mater.*, 1998, **46**, 6053.
- Ringer, S. P., Hono, K., Sakurai, T. and Polmear, I. J., *Scripta mater.*, 1997, **36**, 517.
- Jantzen, T., Fries, S. G., Harmelin, M. G. and Foudot, F., in *Proceedings of CALPHAD XXVIII*, Grenoble, May, 1999.
- Lim, M. S., Tibballs, J. E. and Rossitter, P. L., *Z. Metallk.*, 1997, **88**, 162.
- Software development by Roar Kilaas, National Center for Electron Microscopy (NCEM), Lawrence Berkeley National Laboratory, Berkeley, CA.
- Pennycook, S. J. and Jesson, D. E., *Phys. Rev. Lett.*, 1990, **64**, 938–941.
- Pennycook, S. J. and Jesson, D. E., *Acta metall. mater.*, 1992, **40**, 149–159.
- Pennycook, S. J. and Nellist, P. D., in *Impact of Electron and Scanning Probe Microscopy on Materials Research*, ed. D. G. Rickerby, U. Valdré and G. Valdré. Kluwer, Dordrecht, 1999, p. 161.
- Gull, S. F. and Skilling, J., *IEE Proc.*, 1984, **F131**, 646.
- McGibbon, A. J. and Pennycook, S. J., in *Proceedings of the 52nd Microscopy Society of America Conference, New Orleans, LA*. San Francisco Press, San Francisco, CA, 1994.
- Ashby, M. F. and Brown, L. M., *Phil. Mag.*, 1963, **8**, 1083.
- Ashby, M. F. and Brown, L. M., *Phil. Mag.*, 1963, **8**, 1649.
- Williams, D. B. and Carter, C. B., *Transmission Electron Microscopy*, Vol. 3. Plenum, New York, 1996.
- Larche, F. C., in *Dislocation in Solids*, Vol. 4, ed. F. R. N. Nabarro. North Holland, Amsterdam, 1979, p. 137.
- Cassada, W. A., Shiflet, G. J. and Jesser, W. A., *Acta metall. mater.*, 1992, **40**, 2.
- Wang, Z. M. and Shiflet, G. J., *Metall. Trans.*, 1996, **27A**, 1599.
- Weatherly, G. C., *Can. Met. Quart.*, 1969, **8**, 105.
- Weatherly, G. C., *Acta metall.*, 1971, **19**, 181.
- Doherty, R. D. and Rajab, K. E., *Acta metall.*, 1989, **37**, 2723.
- Garg, A., Chang, Y. C. and Howe, J. M., *Scripta metall.*, 1990, **24**, 677.
- Howe, J. M., Aaronson, H. I. and Gronsky, R., *Acta metall.*, 1985, **33**, 649.
- Rajab, K. E. and Doherty, R. D., *Acta metall.*, 1989, **37**, 2709.
- Aikin, R. M. and Plichta, M. R., *Acta metall.*, 1990, **38**, 77.
- Howe, J. M., Aaronson, H. I. and Gronsky, R., *Acta metall.*, 1985, **33**, 639.
- Nie, J. F., Aaronson, H. I. and Muddle, B. C., in *Proceedings of the International Conference on Solid-Solid Phase Transformations '99 (JIMIC-3)*, ed. M. Koiwa, K. Otsuka and T. Miyazaki. The Japan Inst. of Metals, 1999, p. 157.
- Muddle, B. C. and Nie, J. F., in *Proceedings of the Inter-*

- national Conference on Solid-Solid Phase Transformations '99 (JIMIC-3)*, ed. M. Koiwa, K. Otsuka and T. Miyazaki. The Japan Inst. of Metals, 1999, p. 1128.
64. Murayama, M. and Hono, K., *Scripta mater.*, 2001, **44**, 701–706.
65. Grovenor, C. R. M., Shollock, B. A. and Knowles, K. M., *J. Physique Coll.*, 1989, **50**(C8), 377.
66. Shollock, B. A., Grovenor, C. R. M. and Knowles, K. M., *Scripta metall.*, 1990, **24**, 1239.
67. Sano, N., Hono, K., Sakurai, T. and Hirano, K., *Scripta metall.*, 1991, **25**, 491.
68. Hono, K., Sano, N., Babu, S. S., Okano, R. and Sakurai, T., *Acta metall. mater.*, 1993, **41**, 829.
69. Howe, J. M., *Phil. Mag. Lett.*, 1994, **70**, 111.
70. Rainforth, W. M., Rylands, L. M. and Jones, H., *Scripta metall.*, 1996, **35**, 261.